

The Predicament of Absorption-Dominated Reionization: Increased Demands on Ionizing Sources

FREDERICK B. DAVIES,¹ SARAH E. I. BOSMAN,¹ STEVEN R. FURLANETTO,² GEORGE D. BECKER,³ AND ANSON D'ALOISIO³

¹*Max-Planck-Institut für Astronomie, Königstuhl 17, D-69117 Heidelberg, Germany*

²*Department of Physics & Astronomy, University of California, Los Angeles, CA 90095, USA*

³*Department of Physics & Astronomy, University of California, Riverside, CA 92521, USA*

ABSTRACT

The reionization epoch concludes when ionizing photons reach every corner of the Universe. Reionization has generally been assumed to be limited primarily by the rate at which galaxies produce ionizing photons, but the recent measurement of a surprisingly short ionizing photon mean free path of $0.75_{-0.45}^{+0.65}$ proper Mpc at $z = 6$ by [Becker et al. \(2021\)](#) suggests that absorption by residual neutral hydrogen in the otherwise ionized intergalactic medium may play a much larger role than previously expected. Here we show that consistency between this short mean free path and the coeval dark pixel fraction in the Ly α forest requires a cumulative output of $6.1_{-2.4}^{+11}$ ionizing photons per baryon by reionization's end. This represents a dramatic increase in the ionizing photon budget over previous estimates, greatly exacerbating the tension with measurements of the ionizing output from galaxies at later times. Translating this constraint into the instantaneous ionizing production from galaxies in our model, we find $\log_{10} f_{\text{esc}} \xi_{\text{ion}} / (\text{erg}/\text{Hz})^{-1} = 25.02_{-0.21}^{+0.45}$ at $z \sim 6$. Even with optimistic assumptions about the ionizing production efficiency of early stellar populations, and assuming the galaxy luminosity function extends to extremely faint sources ($M_{\text{UV}} \leq -11$), complete reionization requires the escape fraction of ionizing photons to exceed 20% across the galaxy population. This is far larger than observed in any galaxy population at lower redshifts, requiring rapid evolution in galaxy properties after the first billion years of cosmic time. This tension cannot be completely relieved within existing observational constraints on the hydrogen neutral fraction and mean free path.

1. INTRODUCTION

The epoch of reionization is one of the landmark events in the early history of galaxy formation, during which hydrogen in the intergalactic medium (IGM) – which had been neutral since cosmological recombination at $z \sim 1100$ – was ionized by early galaxies. The measured transmission of Ly α photons through the IGM suggests that reionization was complete by $z \sim 5$ – 6 ([Bosman et al. 2018](#); [Eilers et al. 2018](#); [Yang et al. 2020a](#)), but much is still unknown about the process.

The reionization history is fundamentally connected to the evolution of the sources and sinks of ionizing photons across cosmic time. The sources are thought to be star-forming galaxies (e.g. [Robertson et al. 2015](#)), whose populations have been catalogued via their (non-ionizing) UV luminosity functions (LFs) up to $z \sim 10$ (e.g. [Bouwens et al. 2021](#)). The sinks are thought to

be dense clumps of IGM gas that can shield themselves from ionizing radiation and remain neutral ([Miralda-Escudé et al. 2000](#)) even after their volume has been reionized. These clumps manifest as Lyman-limit systems, and their cumulative opacity defines the “mean free path” λ of ionizing photons in the later Universe (e.g. [Songaila & Cowie 2010](#)). The mean free path can be measured directly via the average attenuation observed in stacked quasar spectra ([Prochaska et al. 2009](#); [Worseck et al. 2014](#)).

In most reionization models, the absorption of ionizing photons is assumed to be modest, requiring only ~ 1 – 3 ionizing photons per baryon (e.g. [Gnedin 2008](#); [Finlator et al. 2012](#)). In that case, the observed LF evolution is consistent with reionization completing at $z \sim 6$, provided the escape fraction of ionizing photons, f_{esc} from these galaxies is somewhat larger ($\gtrsim 10\%$) ([Robertson et al. 2015](#)) than that measured directly in later galaxies (e.g. [Pahl et al. 2021](#)).

Recently, the mean free path at $z \sim 6$ has been measured by [Becker et al. \(2021, henceforth B21\)](#) to be $\lambda = 0.75_{-0.45}^{+0.65}$ proper Mpc ($5.25_{-3.15}^{+4.55}$ comoving Mpc),

Corresponding author: Frederick B. Davies
davies@mpia.de

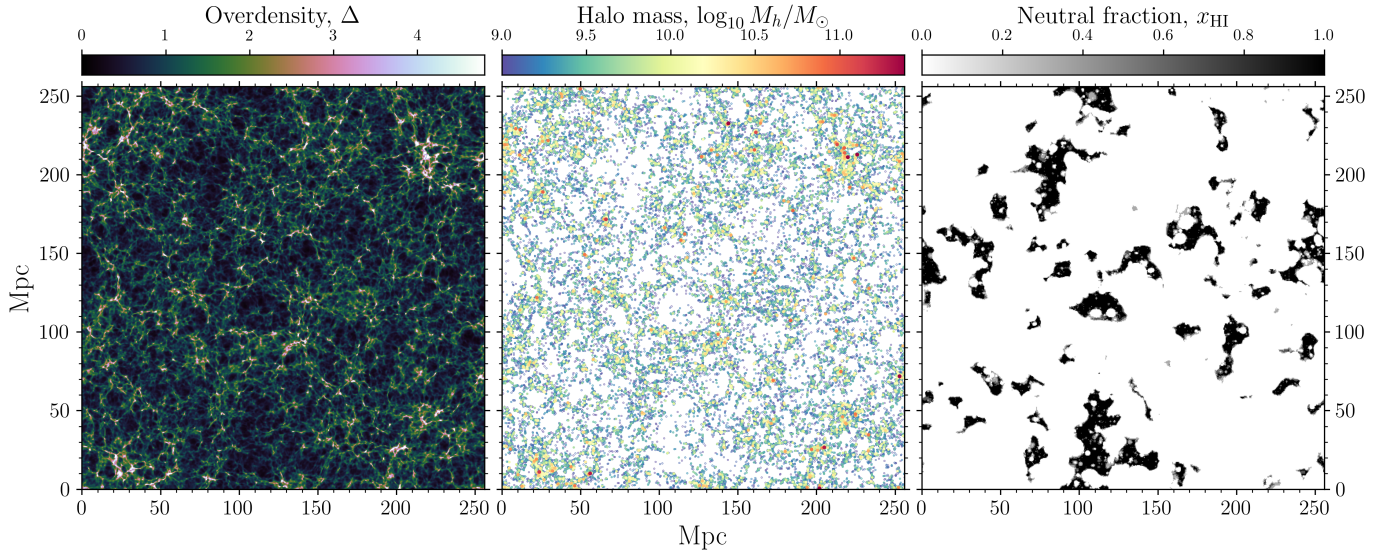


Figure 1. Slice (1.5 Mpc-thick) through our fiducial simulation with $L_{\text{box}} = 256$ Mpc, $\lambda = 5.25$ Mpc, and $M_{\text{min}} = 10^9 M_{\odot}$, matched to the dark pixel fraction 84% confidence upper limit on the volume-fraction of neutral hydrogen at $z = 5.9$ from McGreer et al. (2015). Left: matter overdensity. Middle: dark matter halo distribution, color- and size-coded by mass. Right: hydrogen neutral fraction.

far shorter than the extrapolation from previous measurements at $z \lesssim 5$ using a similar method (Worseck et al. 2014). In this Letter, we investigate the implications of this short mean free path for the reionization epoch using the semi-numerical method of Davies & Furlanetto 2021. We find that the short mean free path implies a dramatic increase in the number of emitted ionizing photons required to reionize the Universe. This in turn requires a substantial increase in the ionizing efficiency of galaxies at $z > 6$ such that their intrinsic properties differ significantly from lower-redshift galaxies.

We adopt a Planck Collaboration et al. (2020) cosmology with $(h, \Omega_m, \Omega_{\Lambda}, \Omega_b, \sigma_8, n_s) = (0.6736, 0.3153, 0.6847, 0.0493, 0.8111, 0.9649)$, and use comoving distances unless specified otherwise.

2. SIMULATION METHOD

To simulate the effect of a short mean free path on reionization, we use the semi-numerical method of Davies & Furlanetto (2021), consisting of a modified version of the 21cmFAST code (Mesinger et al. 2011). The simulations start with cosmological initial conditions (ICs) in a volume of size L_{box} with N_{IC} cells on a side. We then evolve the density field via the Zel’dovich approximation (Zel’dovich 1970) at a coarsened resolution with N_{ev} cells on a side. We employ the halo-filtering methodology of Mesinger & Furlanetto (2007) to identify dark matter halos and evolve their positions using the Zel’dovich displacement field. Our fiducial

simulations adopt $L_{\text{box}} = 256$ Mpc, $N_{\text{IC}} = 4096$, and $N_{\text{ev}} = 512$, so that $L_{\text{cell}} = 0.5$ Mpc. We explore a range of L_{box} from 128 to 512 Mpc at fixed $N_{\text{IC}} = 4096$ and evolved $L_{\text{cell}} = 0.5$ Mpc¹. To limit numerical noise in the halo distribution we adopt a minimum halo mass M_{min} corresponding to ~ 100 mean density IC cells, so each L_{box} has a corresponding M_{min} .

We assume that the mass of material ionized by a halo, in the absence of absorption, is related to its mass via

$$M_{\text{ion}} = \zeta M_h, \quad (1)$$

This ζ is the product of several parameters of stars in early galaxies,

$$\zeta = f_{\text{esc}} f_* N_{\gamma/b}^*, \quad (2)$$

where f_* is the fraction of the halo’s baryons which formed stars and $N_{\gamma/b}^*$ is the (integrated) number of ionizing photons emitted per stellar baryon (Furlanetto et al. 2004).

We employ two different prescriptions for ζ . The first assumes that $\zeta = \zeta_0$ is constant as a function of halo mass, i.e. $M_{\text{ion}} \propto M_h$. This model is motivated by simplicity and by its use in many past works. Our fiducial prescription for ζ assumes a double power-law functional form,

$$\zeta(M_h) = \zeta_0 \frac{(M_0/M_{\text{peak}})^{-\gamma_{\text{lo}}} + (M_0/M_{\text{peak}})^{-\gamma_{\text{hi}}}}{(M_h/M_{\text{peak}})^{-\gamma_{\text{lo}}} + (M_h/M_{\text{peak}})^{-\gamma_{\text{hi}}}}, \quad (3)$$

¹ We find little difference for $L_{\text{cell}} = 0.25$ or 1.0 Mpc.

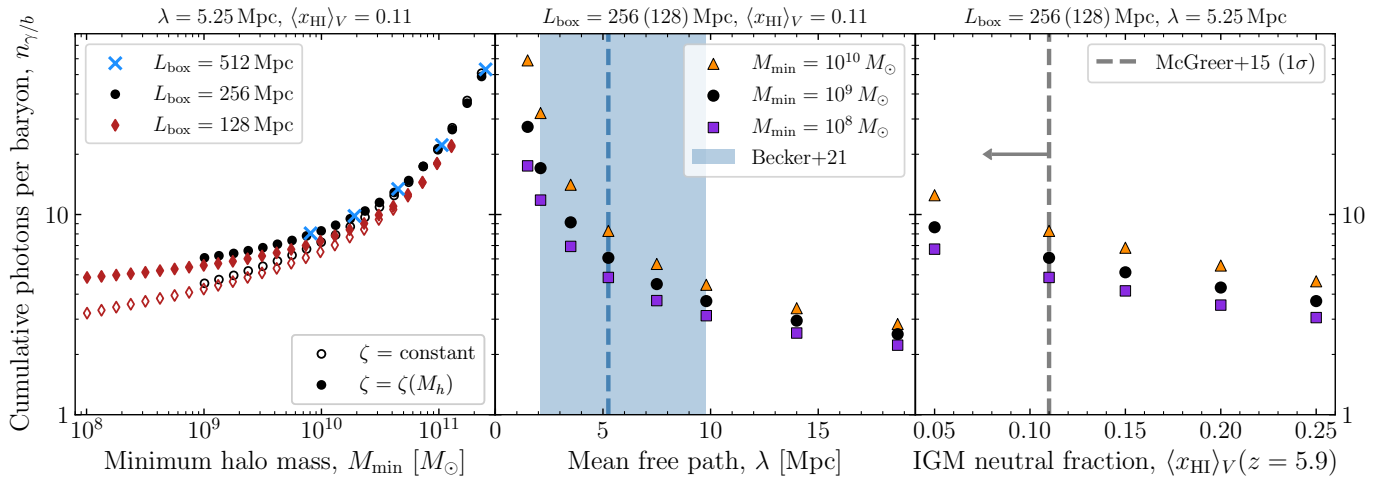


Figure 2. Number of ionizing photons per baryon required to reionize the Universe in our simulations (points). Left: dependence on minimum halo mass, simulation box size, and ζ model. Middle: dependence on mean free path. Due to resolution limitations, simulations with $M_{\min} = 10^8 M_{\odot}$ have $L_{\text{box}} = 128$ Mpc. The B21 mean free path constraint is shown by the blue shaded region. Right: dependence on the volume-averaged neutral fraction at $z = 5.9$. The McGreer et al. (2015) 84% confidence upper limit is shown by the vertical dashed line.

where ζ_0 is a normalization factor applied at a halo mass M_0 , $\gamma_{\text{lo}} = 0.49$ and $\gamma_{\text{hi}} = -0.61$ are effective power-law indices at low and high mass, respectively, and $M_{\text{peak}} = 2.8 \times 10^{11} M_{\odot}$ is a transition mass between the two. This form (and the corresponding parameters) were originally chosen by Mirocha et al. (2017) to characterize the relationship between star formation and halo accretion required to reproduce observed UV LFs at $z = 6-8$ (see also Mirocha 2020). Note that we apply this functional form to the ratio between the *total* number of stars formed and the halo *mass* but in practice the shapes of the two relations should be very similar (Furlanetto et al. 2017). The shape can be interpreted as accounting for a suppression of star formation at low halo masses due to supernova feedback, and at high halo masses due slow gas cooling or AGN feedback (Furlanetto et al. 2017).

We use the “MFP- $\epsilon(r)$ ” approach from Davies & Furlanetto (2021) to compute the ionization topology in the presence of absorption. The standard framework for semi-numerical reionization simulations relies on a photon-counting argument, whereby a region is ionized if the number of ionizing photons produced inside it exceeds the number of hydrogen atoms. This argument is typically applied to a single cell at the center of the region (e.g. Zahn et al. 2011). Davies & Furlanetto (2021) showed that this central cell calculation is equivalent to integrating the ionizing flux, enabling distance-dependent absorption to be efficiently included. In the MFP- $\epsilon(r)$ approach, the ionization criterion on scale R

is given by

$$\int_0^{\infty} \langle \zeta f_{\text{coll}} \Delta \rangle_r W(r; R, \lambda) 4\pi r^2 dr > \langle \Delta(< R) \rangle, \quad (4)$$

where Δ is the overdensity relative to the cosmic mean, f_{coll} is the fraction of matter in halos above the minimum mass for galaxies to form, $\langle \zeta f_{\text{coll}} \Delta \rangle_r$ is averaged within the spherical shell at radius r , and $W(r; R, \lambda)$ is a spherical top-hat filter of size R in real space with an exponential attenuation factor $e^{-r/\lambda}$ to account for absorption in the ionized gas. In Figure 1, we show an example of the evolved density field, halo distribution, and neutral fraction field of our fiducial simulation.

Finally, we note that semi-numerical simulations that use a real-space filter to compute the ionization topology are known to suffer from photon non-conservation (e.g. Zahn et al. 2007) at the $\lesssim 20\%$ level, peaking when ionized bubbles first overlap and weakening towards the later stages of reionization (Hutter 2018). We expect a similar effect to be present in our adopted method, but we note that the uncertainty in the observed mean free path is far larger than 20% and so defer a quantitative comparison to radiative transfer simulations to future work.

3. THE IONIZING PHOTON BUDGET

We aim to constrain the number of ionizing photons that must have been emitted during reionization given the short $z \sim 6$ mean free path measured by B21. We make the simplifying assumption that the mean free path prior to $z = 6$ is constant; in reality, it is likely shorter at earlier times, requiring even more ionizing

photons to complete the process. We then require that the IGM neutral fraction at $z \sim 6$ be consistent with the Ly α dark pixel fraction measurement of [McGreer et al. \(2015\)](#), who found a volume-averaged neutral fraction $\langle x_{\text{HI}} \rangle_V(z = 5.9) < 0.11$ at 84% confidence. We thus tune ζ_0 for each simulation to match $\langle x_{\text{HI}} \rangle_V(z = 5.9) = 0.11$, and also explore variations of this value. The resulting mass-averaged IGM neutral fraction in the simulations is $\langle x_{\text{HI}} \rangle_M \sim 6\%$. In this work we conservatively consider reionization to be ‘‘completed’’ at this point – however, vestiges of incomplete reionization may be detectable at later times in the Ly α forest ([Kulkarni et al. 2019](#); [Keating et al. 2020](#); [Nasir & D’Aloisio 2020](#), [Bosman et al. in prep.](#)) or in future 21 cm measurements ([Raste et al. 2021](#)).

We quantify the ionizing photon budget by the cumulative number of ionizing photons per baryon,

$$n_{\gamma/b} = \frac{n_{\text{ion}}}{\bar{n}_b} = \langle \zeta f_{\text{coll}} \rangle, \quad (5)$$

where n_{ion} is the number density of all ionizing photons ever emitted by galaxies and \bar{n}_b is the mean baryon density. The product $\langle \zeta f_{\text{coll}} \rangle$ represents the average over any halo mass dependence of ζ . Our fiducial simulation with $L_{\text{box}} = 256$ Mpc, $M_{\text{min}} = 10^9 M_{\odot}$, $\langle x_{\text{HI}} \rangle_V(z = 5.9) = 0.11$, and the double power-law ζ model gives $n_{\gamma/b} = 6.1^{+11}_{-2.4}$, with uncertainty from the [B21](#) mean free path measurement alone. The central value is ~ 2 – 6 times larger than typical estimates from earlier models (e.g. [Gnedin 2008](#); [Finlator et al. 2012](#)).

In [Figure 2](#) we show how $n_{\gamma/b}$ varies across the models in our simulation suite. The left panel shows $n_{\gamma/b}$ as a function of M_{min} for the constant ζ models (open symbols) and fiducial double power-law ζ models (solid symbols) for different box sizes; in the smaller (larger) simulations we can resolve less (more) massive halos. Emphasizing lower mass halos, i.e. by decreasing M_{min} or treating ζ as constant, generally requires fewer photons per baryon to complete reionization, because low-mass galaxies are less biased and therefore spatially closer to the voids that are ionized during the later phases of reionization. Their proximity decreases the attenuation from the short mean free path. Meanwhile, the large-scale voids corresponding to the final $\sim 10\%$ ionization of the Universe represent rare, large, underdense structures, so the required photon budget could depend on features on the largest scales. Convergence is achieved for $L_{\text{box}} \gtrsim 200$ Mpc, motivating our focus on a fiducial $L_{\text{box}} = 256$ Mpc simulation suite.

The middle panel of [Figure 2](#) shows the dependence of $n_{\gamma/b}$ on the mean free path. This trend is the dominant one in our simulations, reflecting the importance of the mean free path for the end stages of reionization.

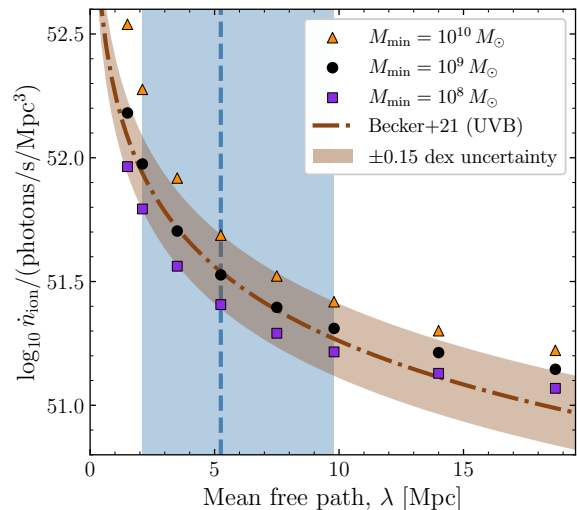


Figure 3. Ionizing emissivity at $z = 5.9$ in our simulations computed via equation (6) as a function of mean free path. The brown dot-dashed curve shows the emissivity that reproduces the mean UV background estimated by [B21](#), with their Γ_{HI} uncertainty shown by the shaded region.

The right panel shows the dependence of $n_{\gamma/b}$ on the assumed IGM neutral fraction at $z = 5.9$. If the neutral fraction at $z = 5.9$ lies significantly below the [McGreer et al. \(2015\)](#) upper limit of 0.11, the required number of photons would increase substantially.

4. IMPLICATIONS FOR REIONIZATION-EPOCH GALAXIES

While the cumulative number of photons per baryon $n_{\gamma/b}$ (and its corresponding ζ prescription) provides a useful cosmological benchmark for reionization studies, it is a time-integrated quantity, which is not trivially related to the galaxy population at any given time. Here we translate our constraint on $n_{\gamma/b}$ to more familiar galaxy properties.

First, we estimate the ionizing emissivity \dot{n}_{ion} from our simulations via differentiating equation (1),

$$\frac{dM_{\text{ion}}}{dt} = \frac{d}{dt}(\zeta M_h) = \zeta \frac{dM_h}{dt} + M_h \frac{d\zeta}{dM_h} \frac{dM_h}{dt}, \quad (6)$$

where $d\zeta/dM_h$ is obtained by differentiating equation (3). We then sum the contribution from every halo i in the simulation and divide by volume to recover \dot{n}_{ion} ,

$$\dot{n}_{\text{ion}} = \frac{1}{L_{\text{box}}^3} \sum_i \frac{(\Omega_b/\Omega_m) \dot{M}_{\text{ion},i}}{\mu m_p}, \quad (7)$$

where Ω_b/Ω_m is the cosmic baryon fraction and μm_p is the average baryon mass. We estimate the halo accretion rate dM_h/dt via the abundance matching-like

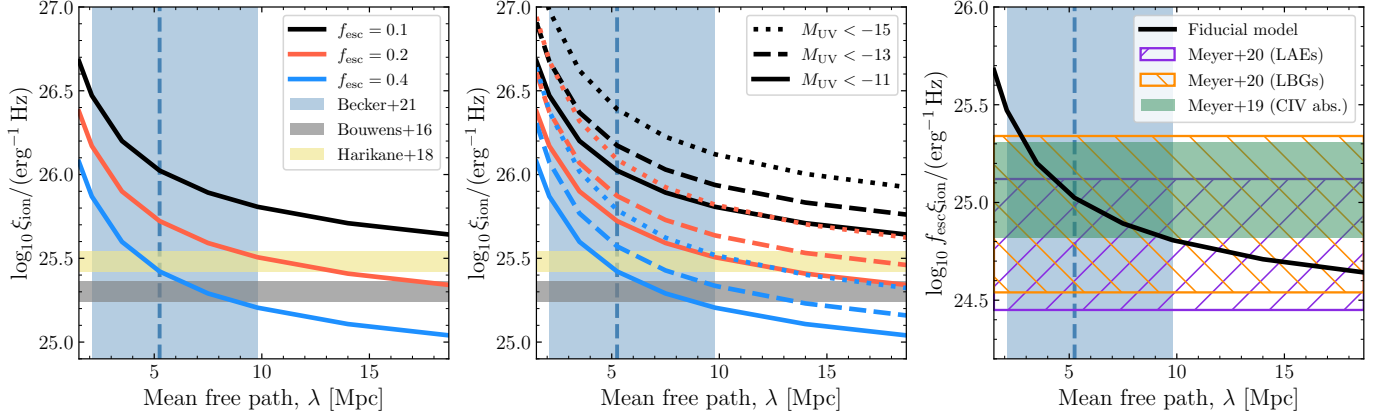


Figure 4. Ionizing photon production and escape (at $z = 5.9$) as a function of mean free path. Left: curves show ξ_{ion} in the fiducial model for varying f_{esc} compared to measurements at $z \sim 4-5$ (Bouwens et al. 2016; Harikane et al. 2018) shown by horizontal bands. Middle: similar to the left panel, but integrating down to different M_{UV} . Right: the black curve shows $f_{\text{esc}}\xi_{\text{ion}}$ in the fiducial model compared to Ly α forest cross-correlation measurements at $z \sim 5-6$ (Meyer et al. 2019, 2020) shown by the horizontal bands and hashes.

procedure described in Furlanetto et al. (2017), wherein dark matter halos grow roughly exponentially in agreement with cosmological simulations (Dekel et al. 2013).

In Figure 3 we show the resulting \dot{n}_{ion} at $z = 5.9$ as a function of mean free path. Our fiducial model ($M_{\text{min}} = 10^9 M_{\odot}$, $\langle x_{\text{HI}} \rangle_V(z = 5.9) = 0.11$) has $\dot{n}_{\text{ion}} = 3.4^{+6.1}_{-1.3} \times 10^{51}$ photons/s/Mpc 3 , where the uncertainties reflect the 1σ range of λ . The ionizing emissivity can also be estimated independently by requiring that the photoionization rate in the IGM, $\Gamma_{\text{HI}} \propto \dot{n}_{\text{ion}}\lambda$, reproduces the observed mean transmission in the Ly α forest. We show \dot{n}_{ion} determined this way by B21 as the brown dot-dashed curve in Figure 3. The two \dot{n}_{ion} estimates agree remarkably well across the 1σ range of the B21 mean free path measurement, although this agreement may be somewhat accidental, as our halo-galaxy mapping is approximate and the UV background measurement may be somewhat biased by fluctuations present at $z \sim 6$ (Davies & Furlanetto 2016; Davies et al. 2018a; Becker et al. 2018).

The ionizing emissivity is typically parameterized by

$$\dot{n}_{\text{ion}} = f_{\text{esc}}\xi_{\text{ion}}\rho_{\text{UV}}, \quad (8)$$

where ξ_{ion} is the ‘‘ionizing efficiency’’ of the stellar populations, dependent on their metallicity and star formation history, and ρ_{UV} is the integrated UV luminosity density. From \dot{n}_{ion} we can thus estimate the product $f_{\text{esc}}\xi_{\text{ion}}$ via observational constraints on ρ_{UV} at $z \sim 6$. Adopting the best-fit star formation efficiency as a function of halo mass from Mirocha et al. (2017), we estimate that our fiducial $M_{\text{min}} = 10^9 M_{\odot}$ corresponds to $M_{\text{UV}} \sim -11$. We then obtain $\rho_{\text{UV}} = 3.2 \times 10^{26}$ erg/s/Hz/Mpc 3 by integrating the $z \sim 6$ UV LF from Bouwens et al. (2021) down to $M_{\text{UV}} = -11$. The solid

curve in the right panel of Figure 4 shows the resulting $f_{\text{esc}}\xi_{\text{ion}}$ from our fiducial model. Taking into account the mean free path uncertainty alone, we estimate $\log_{10} f_{\text{esc}}\xi_{\text{ion}}/(\text{erg}/\text{Hz})^{-1} = 25.02^{+0.45}_{-0.21}$.

Assuming $f_{\text{esc}} = 0.1$, this corresponds to an ionizing efficiency of $\log_{10} \xi_{\text{ion}}/(\text{erg}/\text{Hz})^{-1} = 26.02^{+0.45}_{-0.21}$, considerably larger than previous measurements of $\log_{10} \xi_{\text{ion}}/(\text{erg}/\text{Hz})^{-1} = 25.24 - 25.36$ for $3.8 < z < 5$ galaxies (Bouwens et al. 2016), $\log_{10} \xi_{\text{ion}}/(\text{erg}/\text{Hz})^{-1} = 25.48 \pm 0.06$ for $z \sim 4.9$ Ly α -emitting galaxies (LAEs; Harikane et al. 2018), and even rare, extremely blue galaxies with $\log_{10} \xi_{\text{ion}}/(\text{erg}/\text{Hz})^{-1} \sim 25.8$ (Bouwens et al. 2016; see also Stark et al. 2017). The left panel of Figure 4 shows that maintaining consistency with either the canonical $\log_{10} \xi_{\text{ion}}/(\text{erg}/\text{Hz})^{-1} \sim 25.2$ or the measured value of 25.5 at $z \sim 5$ requires $f_{\text{esc}} \gtrsim 30\%$ or $\gtrsim 20\%$, respectively. Note that, as mentioned above, these constraints reflect contributions from halos down to $M_{\text{min}} = 10^9 M_{\odot}$, corresponding to $M_{\text{UV}} < -11$. The middle panel of Figure 4 shows that increasing the minimum luminosity of contributing galaxies, where $M_{\text{UV}} = -13$ (-15) corresponds to $M_{\text{min}} = 10^{9.5}$ (10^{10}) M_{\odot} , further increases the required $f_{\text{esc}}\xi_{\text{ion}}$.

Our values of $f_{\text{esc}}\xi_{\text{ion}}$ are consistent with Meyer et al. (2019, 2020) (see also Kakiichi et al. 2018) who measured the ionizing production of $z \gtrsim 5$ galaxies via their correlation with Ly α transmission in background quasar spectra. In the right panel of Figure 4, we compare $f_{\text{esc}}\xi_{\text{ion}}$ in our model to values of $f_{\text{esc}}\xi_{\text{ion}}$ values measured from three independent populations of galaxies: Lyman-break galaxies (LBGs), LAEs, and the hosts of C IV absorption systems. We note, however, that the measurements from LAEs and LBGs rely non-trivially on much larger assumed mean free paths at $z \sim 6$.

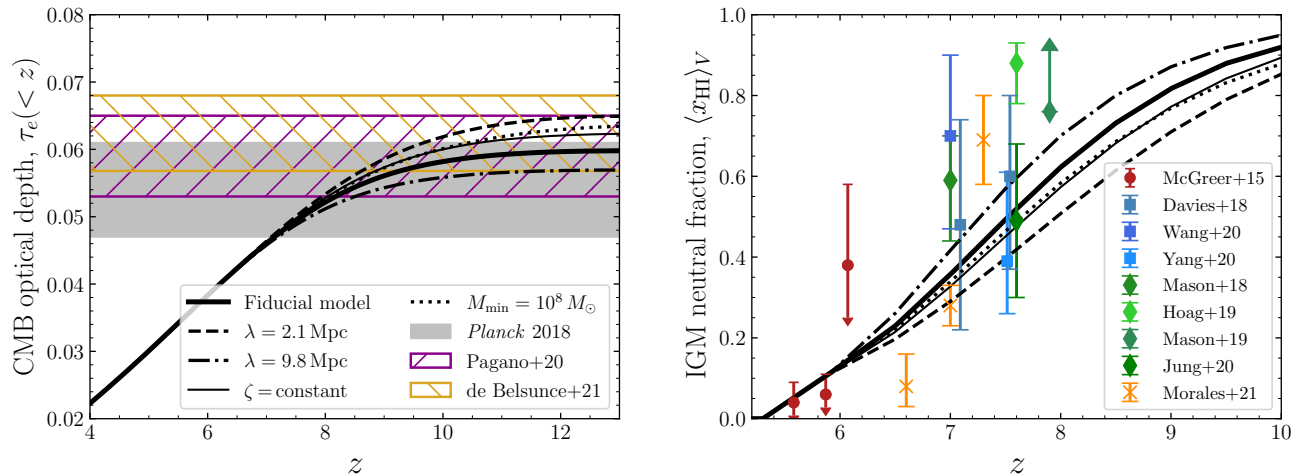


Figure 5. Consistency of our model with observational constraints on reionization. Note that we have not simulated the $z < 5.9$ evolution, but instead assume the increasing mean free path completes reionization by $z = 5.3$. Left: curves show τ_e in the fiducial model (thick solid), $\lambda \pm 1\sigma$ (dashed and dot-dashed), constant ζ (thin solid), and $M_{\text{min}} = 10^8 M_{\odot}$ (dotted). Constraints are shown from Planck Collaboration et al. (2020) (grey shaded), Pagano et al. (2020) (purple hash), and de Belsunce et al. (2021) (yellow hash). Right: evolution of the volume-averaged neutral fraction. Blue squares show constraints from quasar damping wings (Davies et al. 2018b; Wang et al. 2020; Yang et al. 2020b), green diamonds show constraints from Ly α and UV emission from galaxies (Mason et al. 2018, 2019; Hoag et al. 2019; Jung et al. 2020), and orange crosses show a recent constraint from the evolution of the LAE LF (Morales et al. 2021).

Finally, we demonstrate the consistency of our results with measurements of the stellar mass function. We can estimate ξ_{ion} directly from ζ using $f_*(M_h)$ from Mirocha et al. (2017) and estimating $N_{\gamma/b}^*$ using the integral constraint,

$$N_{\gamma/b}^* = \frac{\mathcal{E}_{\text{tot}}|_{z \geq 6}}{M_{*,\text{tot}}|_{z=6}} \xi_{\text{ion}}, \quad (9)$$

where $\mathcal{E}_{\text{tot}}|_{z \geq 6}$ is the energy density in UV photons emitted before $z = 6$, i.e.

$$\mathcal{E}_{\text{tot}}|_{z \geq 6} = \int_{t(z=6)} \int_{L_{\text{min}}} L \Phi(L, t) dL dt \quad (10)$$

and $M_{*,\text{tot}}|_{z=6}$ is the stellar mass density at $z = 6$. Using the best-fit UV LFs from Bouwens et al. (2021) at $z = 5.9, 6.8, 7.9, 8.9$ and Oesch et al. (2018) at $z = 10.2$, we obtain $\mathcal{E}_{\text{tot}}|_{z \geq 6} = 3.9 \times 10^{43}$ erg/Hz/Mpc³, integrating down to our nominal halo mass threshold of $10^9 M_{\odot}$. Dividing our star formation efficiency model by a factor of $1 + \gamma_{\text{lo}}$ to approximately recover the stellar mass-halo mass relation (Furlanetto et al. 2017), this mass threshold corresponds to a minimum stellar mass of $M_{*,\text{min}} \sim 6.6 \times 10^5 M_{\odot}$, implying a mass-to-light ratio of $\sim 0.12 M_{\odot}/L_{\odot}$ at $M_{*,\text{min}}$. This mass-to-light ratio is consistent with measurements in (much brighter) galaxies at $z \geq 6$ (e.g. McLure et al. 2011). Equations (2) and (9) then require $M_{*,\text{tot}}|_{z=6} = 8.8 \times 10^6 M_{\odot}/\text{Mpc}^3$ to match our constraints on $f_{\text{esc}} \xi_{\text{ion}}$, which falls squarely between faint-end extrapolations of the stellar mass functions of Bhatawdekar et al. (2019) ($M_{*,\text{tot}}|_{z=6} =$

$1.1 \times 10^7 M_{\odot}/\text{Mpc}^3$) and Song et al. (2016) ($M_{*,\text{tot}}|_{z=6} = 4.6 \times 10^6 M_{\odot}/\text{Mpc}^3$). Thus our constraints are not in tension with extrapolations of the $z \geq 6$ luminosity and stellar mass functions.

We therefore find that reionization-era galaxies must be producing or leaking ionizing photons with efficiencies a factor 2–3 times higher than even the most optimistic observational estimates to match the $\langle x_{\text{HI}} \rangle_V$ constraint at $z = 5.9$. The tension could be eased if the UV LF is much steeper at $z \sim 6$, e.g. with a faint-end slope at the 2σ limit from Bouwens et al. (2021) the required $f_{\text{esc}} \xi_{\text{ion}}$ would decrease by a factor of two. A strongly declining f_{esc} with halo mass could also decrease the required photon budget; the constant ζ model, implying $f_{\text{esc}} \propto M_h^{-0.49}$, decreases $n_{\gamma/b}$ by $\sim 30\%$. Cain et al. (2021) have similarly explored the ionizing budget requirements of reionization with a short mean free path using radiative transfer simulations that include a simulation-calibrated sub-grid model for small-scale gas clumping. Their fiducial simulation assumes that every halo has the same ionizing luminosity, placing even more emphasis on the faintest galaxies. Their ionizing photon budget at $z = 5.9$ of $n_{\gamma/b} \sim 2.2$ is nevertheless within $\sim 10\%$ of our constant ζ model when run with values of $\langle x_{\text{HI}} \rangle_V = 0.2$ and $\lambda = 10$ Mpc similar to their model (at the $\sim +2\sigma$ and $\sim +1\sigma$ of current observations, respectively), which gives $n_{\gamma/b} \approx 2.3$.

5. CONCLUSION

In this work, we have explored the consequences of a short mean free path of ionizing photons (as measured by B21) on the ionizing photon budget of the reionization epoch. Using the new semi-numerical method of Davies & Furlanetto (2021), we found that their mean free path of $0.75_{-0.45}^{+0.65}$ proper Mpc implies a cumulative ionizing photon budget of $6.1_{-2.4}^{+11}$ photons per baryon to reproduce the 1σ upper limit on the $z = 5.9$ IGM neutral fraction of $\langle x_{\text{HI}} \rangle_V < 0.11$ from McGreer et al. (2015). The large number of required photons is linked to the distance that the photons must travel from sources to the last remaining neutral voids.

We translated our constraint on the cumulative number of photons per baryon into the instantaneous emission properties of reionization-epoch galaxies, finding an implied ionizing production rate of $\log_{10} f_{\text{esc}} \xi_{\text{ion}} / (\text{erg/Hz})^{-1} = 25.02_{-0.21}^{+0.45}$. Even assuming that reionization-epoch galaxies are substantially more efficient at producing ionizing photons than their lower-redshift counterparts ($\log_{10} \xi_{\text{ion}} / (\text{erg/Hz})^{-1} = 25.5$), and integrating the UV luminosity function down to extremely faint magnitudes ($M_{\text{UV}} \leq 11$), we conservatively require an average $f_{\text{esc}} > 20\%$ from $z > 6$ galaxies, more than three times larger than measurements in $z = 3$ galaxies ($f_{\text{esc}} \sim 6\%$; Pahl et al. 2021). A more conventional production rate of $\log_{10} \xi_{\text{ion}} / (\text{erg/Hz})^{-1} = 25.2$ requires an even more extreme $f_{\text{esc}} > 30\%$. Qualitatively, a “photon budget crisis” occurs because the B21 mean free path measurement at $z \sim 6$ implies that ionizing photon sinks are far more numerous than previously assumed.

Our models are nevertheless consistent with available reionization history constraints, as shown in Figure 5, and with measurements of the UV LF and stellar mass density (see § 4). Astrophysical constraints on the ionized fraction at $z \sim 7$ (Fig. 5, right) may point towards somewhat more rapid reionization, but our models have

more gradual histories because IGM absorption becomes increasingly important later in the process.

Future observations will help resolve, or further exacerbate, this ionizing photon budget deficit. Tighter constraints on the mean free path at $z \gtrsim 5.5$, with improved quasar bias modeling, would most directly improve the constraints. Improved upper limits on the dark pixel fraction at $z \sim 6$ would provide a more robust limit on the IGM neutral fraction. Deeper observations of high-redshift galaxies with *JWST* will deliver precise UV LFs to fainter magnitudes, potentially locating a “turnover” corresponding to the onset of star formation in low mass halos. The depth and wavelength coverage of *JWST* spectroscopy will enable direct measurements of ξ_{ion} (and possibly f_{esc}) from nebular lines, and test for consistency with our models.

We thank Joseph Hennawi and the ENIGMA group at UCSB/Leiden for access to the computing resources used in this work.

SEIB acknowledges funding from the European Research Council (ERC) under the European Union’s Horizon 2020 research and innovation programme (grant agreement No. 740246 “Cosmic Gas”).

This work was supported by the National Science Foundation through award AST-1812458. In addition, this work was directly supported by the NASA Solar System Exploration Research Virtual Institute cooperative agreement number 80ARC017M0006. We also acknowledge a NASA contract supporting the “WFIRST Extragalactic Potential Observations (EXPO) Science Investigation Team” (15-WFIRST15-0004), administered by GSFC. This material is based upon work supported by the National Science Foundation under Grant Nos. 1636646 and 1836019, the Gordon and Betty Moore Foundation, and institutional support from the HERA collaboration partners.

REFERENCES

- Becker, G. D., D’Aloisio, A., Christenson, H. M., et al. 2021, arXiv e-prints, arXiv:2103.16610
- Becker, G. D., Davies, F. B., Furlanetto, S. R., et al. 2018, *ApJ*, 863, 92
- Bhatawdekar, R., Conselice, C. J., Margalef-Bentabol, B., & Duncan, K. 2019, *MNRAS*, 486, 3805
- Bosman, S. E. I., Fan, X., Jiang, L., et al. 2018, *MNRAS*, 479, 1055
- Bouwens, R. J., Smit, R., Labbé, I., et al. 2016, *ApJ*, 831, 176
- Bouwens, R. J., Oesch, P. A., Stefanon, M., et al. 2021, arXiv e-prints, arXiv:2102.07775
- Cain, C., D’Aloisio, A., Gangolli, N., & Becker, G. D. 2021, submitted
- Davies, F. B., Becker, G. D., & Furlanetto, S. R. 2018a, *ApJ*, 860, 155
- Davies, F. B., & Furlanetto, S. R. 2016, *MNRAS*, 460, 1328
- . 2021, arXiv e-prints, arXiv:2103.09821
- Davies, F. B., Hennawi, J. F., Bañados, E., et al. 2018b, *ApJ*, 864, 142

- de Belsunce, R., Gratton, S., Coulton, W., & Efstathiou, G. 2021, arXiv e-prints, arXiv:2103.14378
- Dekel, A., Zolotov, A., Tweed, D., et al. 2013, *MNRAS*, 435, 999
- Eilers, A.-C., Davies, F. B., & Hennawi, J. F. 2018, *ApJ*, 864, 53
- Finlator, K., Oh, S. P., Özel, F., & Davé, R. 2012, *MNRAS*, 427, 2464
- Furlanetto, S. R., Mirocha, J., Mebane, R. H., & Sun, G. 2017, *MNRAS*, 472, 1576
- Furlanetto, S. R., Zaldarriaga, M., & Hernquist, L. 2004, *ApJ*, 613, 1
- Gnedin, N. Y. 2008, *ApJL*, 673, L1
- Harikane, Y., Ouchi, M., Shibuya, T., et al. 2018, *ApJ*, 859, 84
- Hoag, A., Bradač, M., Huang, K.-H., et al. 2019, arXiv e-prints, arXiv:1901.09001
- Hutter, A. 2018, *MNRAS*, 477, 1549
- Jung, I., Finkelstein, S. L., Dickinson, M., et al. 2020, *ApJ*, 904, 144
- Kakiichi, K., Ellis, R. S., Laporte, N., et al. 2018, *MNRAS*, 479, 43
- Keating, L. C., Weinberger, L. H., Kulkarni, G., et al. 2020, *MNRAS*, 491, 1736
- Kulkarni, G., Worseck, G., & Hennawi, J. F. 2019, *MNRAS*, 488, 1035
- Mason, C. A., Treu, T., Dijkstra, M., et al. 2018, *ApJ*, 856, 2
- Mason, C. A., Fontana, A., Treu, T., et al. 2019, *MNRAS*, 485, 3947
- McGreer, I. D., Mesinger, A., & D’Odorico, V. 2015, *MNRAS*, 447, 499
- McLure, R. J., Dunlop, J. S., de Ravel, L., et al. 2011, *MNRAS*, 418, 2074
- Mesinger, A., & Furlanetto, S. 2007, *ApJ*, 669, 663
- Mesinger, A., Furlanetto, S., & Cen, R. 2011, *MNRAS*, 411, 955
- Meyer, R. A., Bosman, S. E. I., Kakiichi, K., & Ellis, R. S. 2019, *MNRAS*, 483, 19
- Meyer, R. A., Kakiichi, K., Bosman, S. E. I., et al. 2020, *MNRAS*, 494, 1560
- Miralda-Escudé, J., Haehnelt, M., & Rees, M. J. 2000, *ApJ*, 530, 1
- Mirocha, J. 2020, *MNRAS*, 499, 4534
- Mirocha, J., Furlanetto, S. R., & Sun, G. 2017, *MNRAS*, 464, 1365
- Morales, A., Mason, C., Bruton, S., et al. 2021, arXiv e-prints, arXiv:2101.01205
- Nasir, F., & D’Aloisio, A. 2020, *MNRAS*, 494, 3080
- Oesch, P. A., Bouwens, R. J., Illingworth, G. D., Labbé, I., & Stefanon, M. 2018, *ApJ*, 855, 105
- Pagano, L., Delouis, J. M., Mottet, S., Puget, J. L., & Vibert, L. 2020, *A&A*, 635, A99
- Pahl, A. J., Shapley, A., Steidel, C. C., Chen, Y., & Reddy, N. A. 2021, arXiv e-prints, arXiv:2104.02081
- Planck Collaboration, Aghanim, N., Akrami, Y., et al. 2020, *A&A*, 641, A6
- Prochaska, J. X., Worseck, G., & O’Meara, J. M. 2009, *ApJL*, 705, L113
- Raste, J., Kulkarni, G., Keating, L. C., et al. 2021, arXiv e-prints, arXiv:2103.03261
- Robertson, B. E., Ellis, R. S., Furlanetto, S. R., & Dunlop, J. S. 2015, *ApJL*, 802, L19
- Song, M., Finkelstein, S. L., Ashby, M. L. N., et al. 2016, *ApJ*, 825, 5
- Songaila, A., & Cowie, L. L. 2010, *ApJ*, 721, 1448
- Stark, D. P., Ellis, R. S., Charlot, S., et al. 2017, *MNRAS*, 464, 469
- Wang, F., Davies, F. B., Yang, J., et al. 2020, *ApJ*, 896, 23
- Worseck, G., Prochaska, J. X., O’Meara, J. M., et al. 2014, *MNRAS*, 445, 1745
- Yang, J., Wang, F., Fan, X., et al. 2020a, *ApJ*, 904, 26
- . 2020b, *ApJL*, 897, L14
- Zahn, O., Lidz, A., McQuinn, M., et al. 2007, *ApJ*, 654, 12
- Zahn, O., Mesinger, A., McQuinn, M., et al. 2011, *MNRAS*, 414, 727
- Zel’dovich, Y. B. 1970, *A&A*, 5, 84